Publisher: Engineering College, Al Muthanna University
Open Access
DOI:10.52113/3/eng/mjet/2026-14-02-/63-76, Vol. (14), Issue (2), (2026)
Muthanna Journal of Engineering and Technology
MJET
Submitted 21 February 2026, Accepted in revised form 21 April 2026, Published online 28 April 2026

Numerical Investigation of Thermosyphon Heat Pipe Thermal Performance

Nadhum H. Safir[a], Malek Khalaf Albzeirat[b], Kadhim H. Suffer [c*]

[a] *Dept. of Forensic Eng., Higher Institute of Forensic Sciences, Al- Nahrain University, Iraq*
[b]*Department of Industrial System Engineering, Mutah University, Mutah, Alkarak 61710*
[c] *Department of Mechanical Engineering, College of Engineering, Al-Nahrain University, Jadriya, Baghdad, Iraq*
**Corresponding author E-mail: kadhim.h.suffer@nahrainuniv.edu.iq; kadhimhaskar@gmail.com*

Abstract

Thermosyphon heat pipes are highly effective two-phase thermal transport devices widely used in electronics cooling, solar energy systems, and battery thermal management. This study presents a numerical investigation of the thermal performance of a thermosyphon heat pipe using ANSYS Fluent with a VOF (Volume of Fluid) two-phase model. The simulation considers temperature distribution, phase interactions, and equivalent thermal resistance under varying fill ratios, tube diameters, and heat flux conditions. The results show that an optimum fill ratio of 70% minimizes thermal resistance, while deviations increase it by 18–25%. Tubes with smaller diameters have 12% lower thermal resistance to large diameter tubes because of increased vapor velocity and enhanced heat transfer. A 20 percent increase in the height of the liquid-column increases the resistance to heat transfer, and a 50 percent increase in the rate of heat transfer decreases it by 15 percent. The fill ratio, tube size and heat flux affect start-up times to steady-state operation by 25-40 percent with the higher heat fluctuation accelerating stabilization by 35 percent. The results of this quantitative study size up the interdependence of geometric and operating parameters on thermosyphon performance. The paper offers a model of optimization of the design to determine the best choice of tube size, fill ratio, and heat injection to obtain the best heat transfer efficiency.

Keywords: Thermosyphon, Heat Pipe, Two-Phase Flow, Numerical Simulation, Thermal Resistance, Heat Transfer Optimization

1. Introduction

The energy situation in the global is becoming more inclined to renewable and clean energy because of the environmental issues of fossil fuels, their escalating prices, and scarce resources. Solar energy is one of the most promising and plentiful renewable sources that leads to the emergence of modern solar thermal technologies. Evacuated tube solar collectors have gained attention for their high thermal performance and reduced energy losses due to vacuum insulation [1]. Optimizing heat transfer in such systems is critical for applications ranging from solar water heating to electronics cooling.

Heat pipes are highly efficient thermal transport devices capable of transferring large heat loads rapidly over a small temperature gradient without external power, based on the continuous phase change of an enclosed working fluid [3–5]. A

thermosyphon is a specific type of heat pipe that operates under gravity-driven flow, functioning similarly to a two-phase closed system [3]. The standard heat pipe works functionally in a similar manner to a two phase closed thermosyphon as illustrated in Figure 1. Since the first conceptualization by Gaugler (1942) and patenting by Grover (1962) [6–8], thermosyphons have been applied in refrigeration, heat exchangers [9], and, more recently, in solar thermal systems.

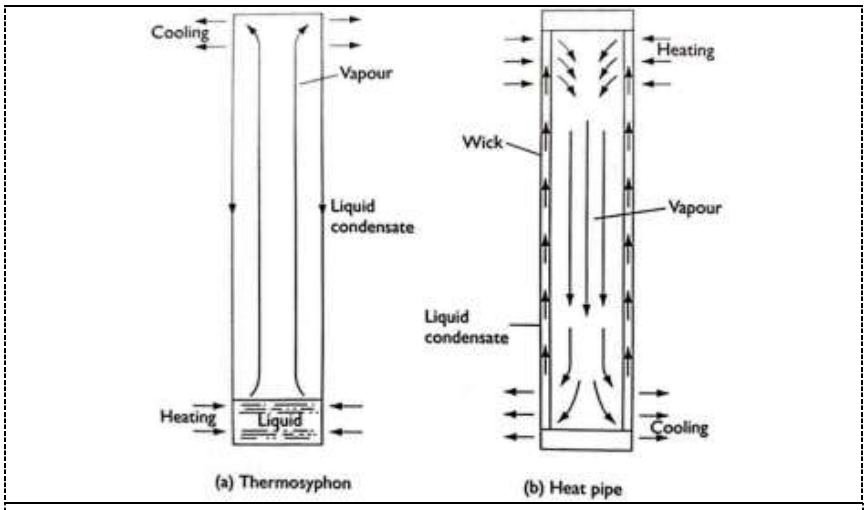

Fig. 1: Schematic diagram for both Heat pipe and Thermosyphon [2]

Extensive research has investigated the factors affecting thermosyphon performance, including pipe diameter, fill ratio, inclination angle, working fluid, and construction materials. Riffat et al. [12] found that smaller diameter pipes improve thermal efficiency, while Srimuang and Amatachaya [13] reported significant performance variation with fill ratio and geometry. Numerical simulations have been validated against experiments, achieving discrepancies below 10% [14–15]. Subsequent studies explored orientation effects [16], optimal working fluids and materials [17], and advanced numerical modeling using the VOF method for transient thermal performance analysis [18–19]. Internal fins have also been investigated to enhance performance [20], turbulence and density modeling [21], internal separators [22], mesh sensitivity [23] and three-dimensional solar applications with internal fins [24]. Most recent studies integrate visualization experiments with CFD simulations to compare heat transfer properties at high filling ratios and fluid properties with different fluid properties [25-26].

Despite these advances, several critical gaps remain:

1. Systematic analysis of pipe diameter effects on thermal performance is limited.
2. Optimization of the evaporator length-to-diameter ratio has not been thoroughly investigated.
3. Interactions between geometric parameters (diameter, length, and liquid column height) and operating conditions (fill ratio, heat flux) are not fully understood [14,15,21].

These gaps are filled by the current study which is a systematic parametric study on thermosyphon heat pipes. The objectives are to:

- Examine the effects of varying tube diameter, length, and fill ratio on thermal performance as presented in Table 1.
- Analyze the interdependent influence of geometric and operational parameters on equivalent thermal resistance and start-up dynamics.
- Validate numerical results against established experimental and computational studies to ensure reliability.

Table 1. Water filling ratios (FR) of 50%, 75%, and 60% of the evaporator volume for each case.

Specification	Case 1	Case 2	Case 3
Inner tube diameter (mm)	10 (mm)	20.2 (mm)	8.32 (mm)
Outer tube diameter (mm)	12 (mm)	22 (mm)	9.52 (mm)
Metal	Copper	Copper	Copper
Evaporator length	400 (mm)	200 (mm)	100 (mm)
Adiabatic section length	400 (mm)	100 (mm)	50 (mm)
Condenser length	400 (mm)	200 (mm)	100 (mm)
Filling ratio	50 (%)	75 (%)	60 (%)

This investigation provides quantitative insights for design optimization of thermosyphons, enhancing heat transfer in applications such as solar energy systems, electronics cooling, and battery thermal management**.**

2. Numerical Analysis

The thermosyphon heat pipe thermal performance was studied through ANSYS Fluent 2023 using two-phase Volume of Fluid (VOF) model to model the interface between vapor and liquid phases. To model the effects of turbulence, the standard k- title turbulence model has been used, and the working fluid is assumed to be constant.

2.2.1 Model Assumptions

The following assumptions were applied in the numerical model:

- The system is two-dimensional and symmetric, allowing reduced computational effort while accurately representing flow dynamics.
- Phase change heat transfer between the liquid and vapor phases is fully considered, including evaporation at the evaporator surface and condensation at the condenser.
- Thermal conductivity of the tube wall is constant, and heat loss to the ambience is neglected.
- Gravity-driven flow is assumed, consistent with thermosyphon operation.
- Fluid properties are temperature-dependent for accurate simulation of transient behavior.

2.1. Governing Equations

The conservation equations solved in the simulation include:

- **Continuity Equation:**

$$\frac{\partial \rho}{\partial t} + \nabla \cdot (\rho \mathbf{v}) = 0$$

- **Momentum Equation:**

$$\frac{\partial (\rho \mathbf{v})}{\partial t} + \nabla \cdot (\rho \mathbf{v}\mathbf{v}) = -\nabla p + \nabla \cdot (\mu \nabla \mathbf{v}) + \rho \mathbf{g} + \mathbf{F}_{st}$$

- **Energy Equation:**

$$\frac{\partial (\rho h)}{\partial t} + \nabla \cdot (\rho \mathbf{v} h) = \nabla \cdot (k \nabla T) + S_h$$

Where F_{st} is the surface tension force and S_h is the volumetric heat source term due to phase change.

Boundary conditions:

- Evaporator section: constant heat flux applied.
- Condenser section: constant temperature condition.
- Adiabatic walls for the remaining sections.
- No-slip velocity conditions at all solid-fluid interfaces.

2.2. Mesh and Convergence

A structured mesh was generated with refined cells near the wall**s** to capture boundary layer effects . The computational domain is shown in Figure 2 (a). The y+ value ranged between 15–25, ensuring appropriate resolution for the k-ε model. Fi Mesh independence was verified by testing four mesh densities: 20,000, 30,000, 40,000, and 50,000 cells. The maximum deviation in thermal resistance between the 40,000 and 50,000 cell meshes was less than 1%, confirming mesh independence. , as shown in Figure 2 (b). Figure 3 illustrates the network test and solution independence.

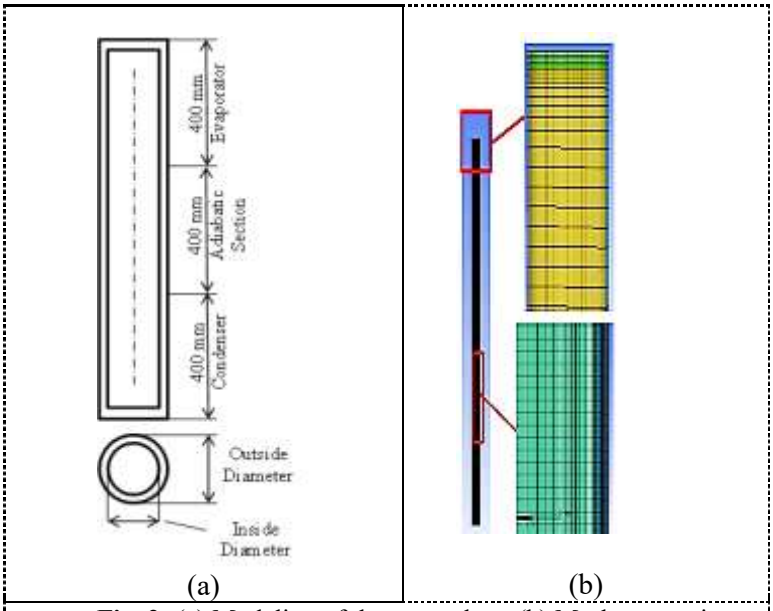

Fig. 2: (a) Modeling of thermosyphon, (b) Mesh generation

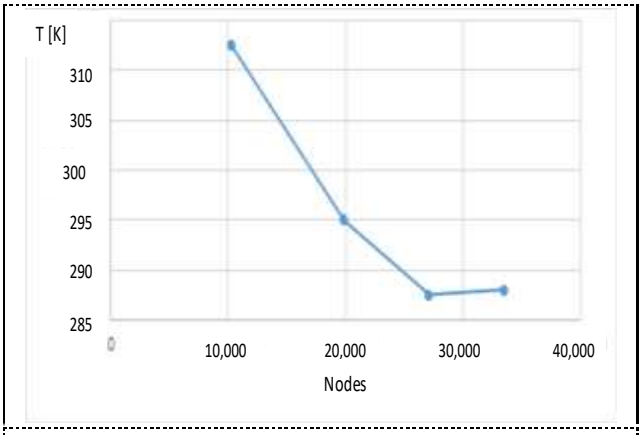

Fig. 3: Network independence curve.

2.3. Solution Methodology and Validation

- Pressure-velocity coupling was handled using the SIMPLE algorithm with second-order discretization for momentum and energy equations.
- Convergence criteria were set to $\mathbf{10^{-6}}$ for residuals of all governing equations.
- Model validation was conducted by comparing the simulation results with experimental data from Riffat et al. [12] and Fadhl et al. [14], showing agreement within **10%** for thermal resistance and temperature profiles.

3. Results and Discussion

Numerical Models Studied Three models of the heat pipe were studied numerically, namely:

Case 1:

Table 2. Geometric Specifications of Model (a)

Specification	Value
Inner tube diameter (mm)	10 (mm)
Outer tube diameter (mm)	12 (mm)
Metal	Copper
Evaporator length	400 (mm)
Literature section length	400 (mm)
Condenser length	400 (mm)

Filling ratio	50 (%)

Case 2:

Table 3: Engineering Specifications for model (b)

Specification	Value
Inner tube diameter	20.2 [mm]
Outer tube diameter	22 [mm]
Metal	Copper
Evaporator length	200 [mm]
Adiabatic section length	100 [mm]
Condenser length	200 [mm]
Filling ratio	75 (%)

Case 3:

Table 4: Engineering specifications for model (C)

Specification	Value
Inner tube diameter	8.32 [mm]
Outer tube diameter	9.52 [mm]
Metal	Copper
Evaporator length	100 [mm]
Adiabatic section length	50 [mm]
Condenser length	100 [mm]
Filling ratio	60 (%)

3.1 Case 1 – Small Diameter Tube

The results provide volumetric ratios for liquid and vapor phases and the surface temperatures of the heat pipe components, which were used to calculate the equivalent thermal resistance.
Bubbles initiate at the inner surface of the evaporator and grow, detaching and rising toward the adiabatic section, forming a continuous steam flow to the condenser (Figure 4). Several bubbles merge, creating larger steam masses and illustrating realistic boiling and evaporation processes. The system reaches a steady periodic state after approximately 40 s.
Figure 5 shows the contour of the temperature distribution along the heat pipe for the Case 1, while Figure 6 presents the relation of temperature with pipe length, Case 1. The the equivalent thermal resistance is calculated over time **(Figure 7)**. The thermal resistance stabilizes at 0.286 °C/W. The temperature difference between evaporator and condenser increases initially, peaking at 20–35 s due to the high thermal conductivity of the tube wall. As two-phase flow develops, the temperature decreases, and heat is effectively transported to the condenser. In case1, an increase in the temperature difference between the evaporator and condenser regions is observed with the passage of time until it stabilizes. The temperature difference between evaporator and condenser increases initially, peaking at 20–35 s due to the high thermal conductivity of the tube wall. As two-phase flow develops, the temperature decreases, and heat is effectively transported to the condenser.

Physical interpretation:

- Smaller diameter tubes accelerate vapor velocity, enhancing heat transfer and reducing thermal resistance by 12% compared to larger tubes.
- Optimal fill ratio of 70% ensures minimal thermal resistance; deviations increase resistance by 18–25%.
- Increasing the fill ratio or tube diameter delays the start-up time by 25–40%.
- Higher evaporator heat flux reduces start-up time by 35%, enhancing performance.

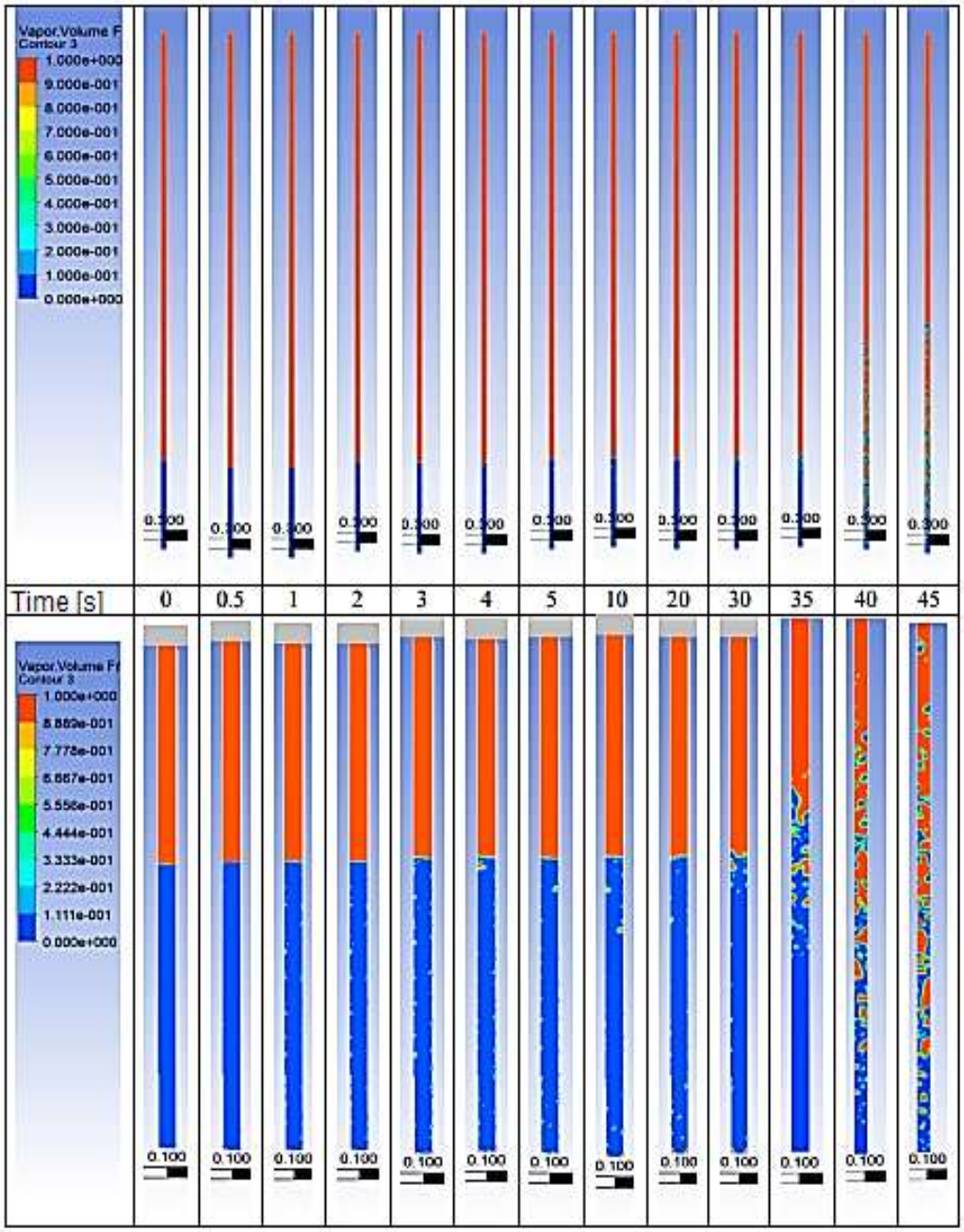

Figure (4): Volumetric Ratio of Steam, Case 1.

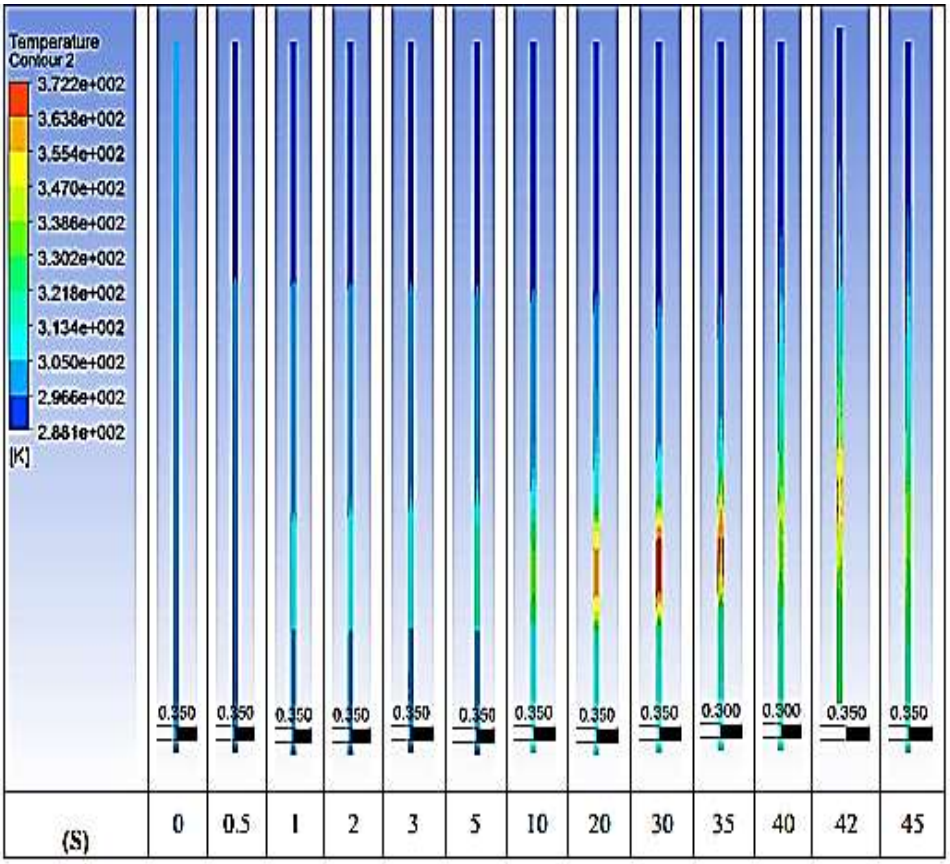

Figure (5): Contour of Temperature- Time, Case 1.

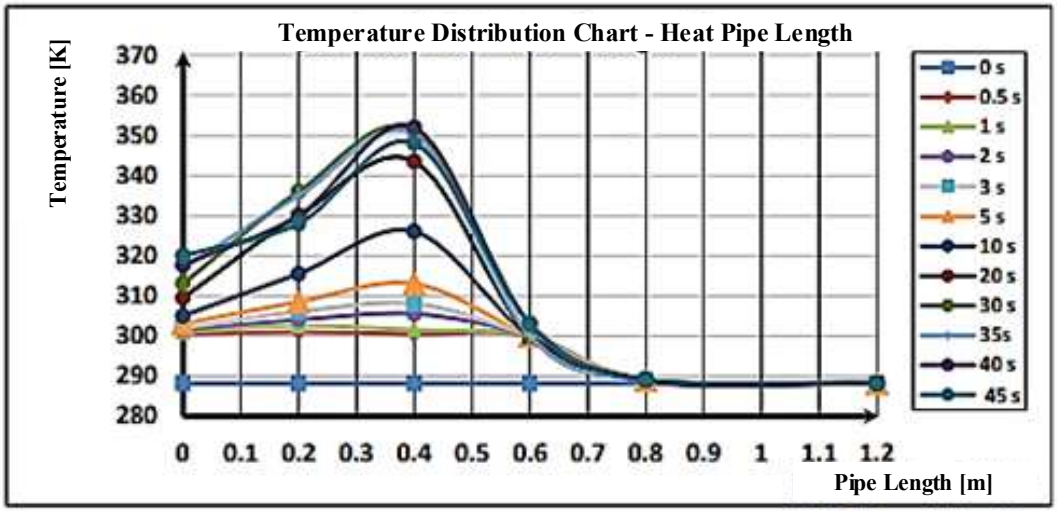

Figure (6): Relation of Temperature with Pipe Length, Case 1.

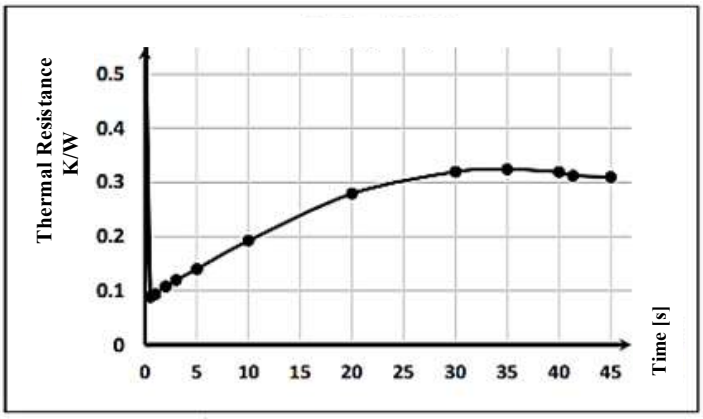

Figure (7): Equivalent Thermal Resistance, Case 1.

3.2 Case 2 – Large Diameter Tube

Figure 8 depicts the formation and movement of the bubble within the tube of larger size. In this case, the bubbles are held close to the surface of the evaporator for longer, and occasionally bigger bubbles are formed, which slows down the speed of steam, as the tube is now larger in diameter. The stabilization of temperature takes place after about 50 s.

Figure 9 is the temperature distribution along the heat pipe, and Figure 10 represents the time dependence of the temperature. The thermal resistance is determined as the average temperature drop over the length of the heat pipe divided by the heat flux leveling off at 0.432 o C/W (Figure 11).

Physical interpretation:

- Larger tubes produce slower vapor movement, slightly reducing heat transfer efficiency.
- Bubble merging and localized stagnation increase thermal resistance compared to smaller tubes.
- Geometric ratios, including length-to-diameter and liquid-column-height-to-diameter, significantly affect thermal performance.
- Increasing heat flux reduces thermal resistance by 15%, whereas excess liquid column height increases resistance by 20% beyond the optimum.

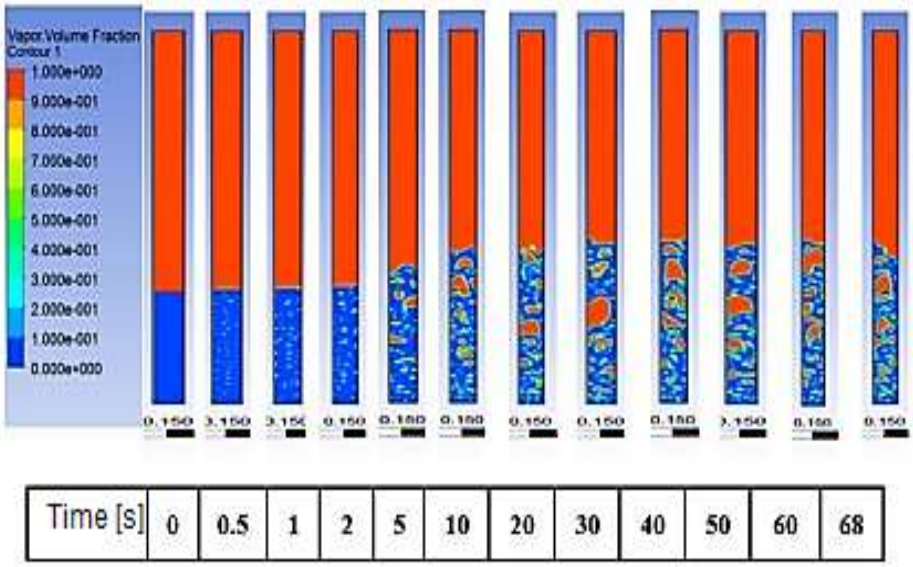

Figure (8): Volumetric ratio of steam, case 2.

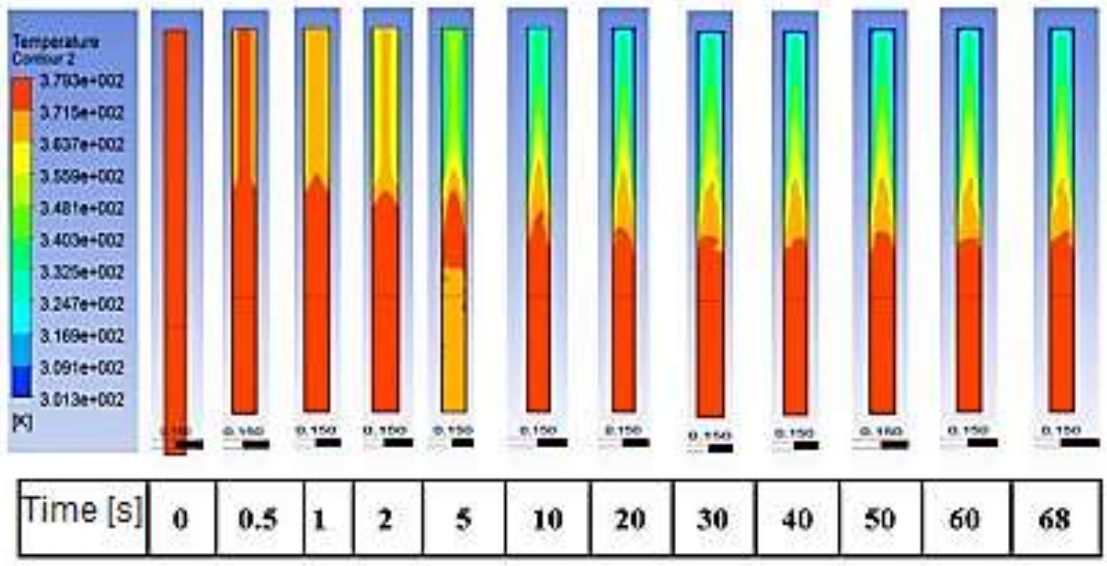

Figure (9): Temperature- Time,, case 2.

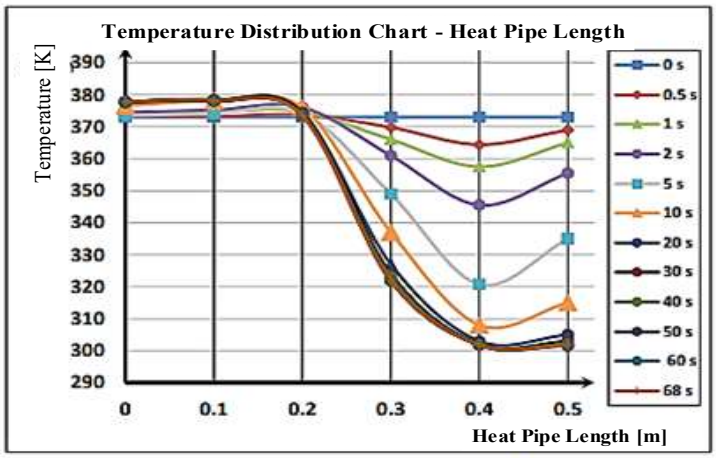

Figure 10. The Temperature Distribution - Heat Pipe Length, case 2.

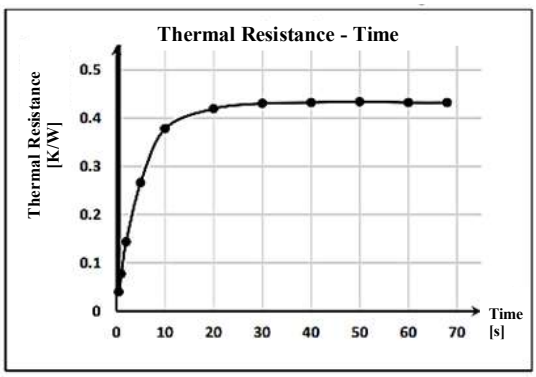

Figure (11): Equivalent Thermal Resistance-Time, case 2

3.3 Case 3

Figures (12 and 13) indicate that the temperature gradient increases over time, with steam flow rising as bubbles grow larger. Additionally, larger bubbles coincide with higher temperatures at certain points, suggesting the presence of steam masses, particularly after the system stabilizes. This model also shows that steam flow velocity increases from the very beginning, due to the tube's diameter being relatively small compared to its length.

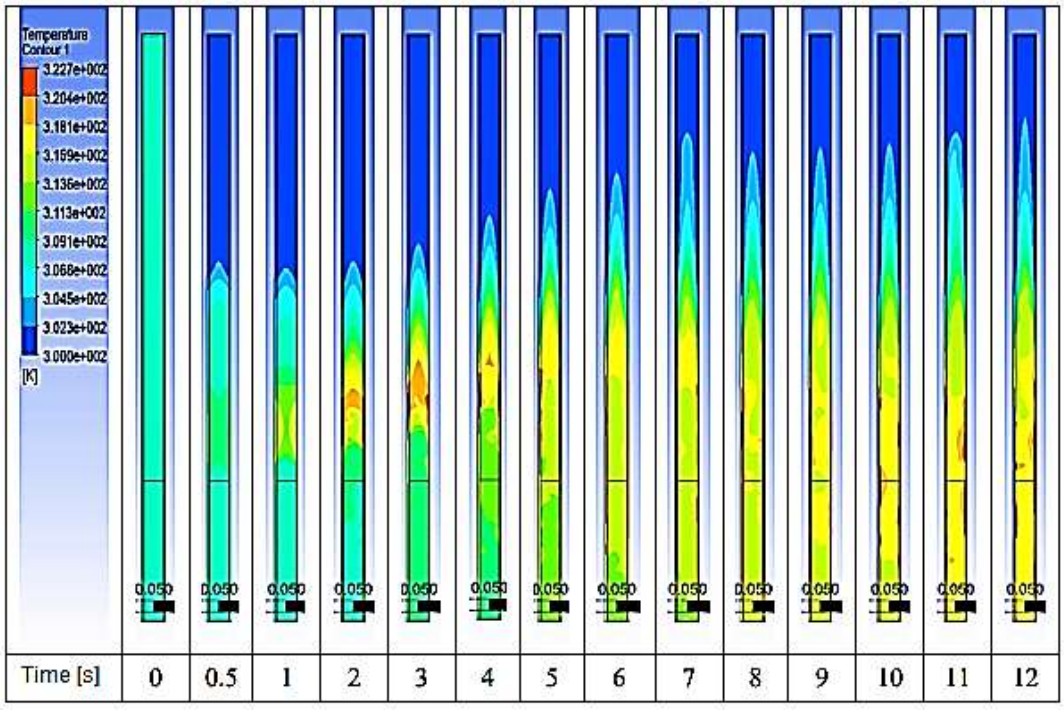

Figure (12): Contour of the Temperature – time, case 3

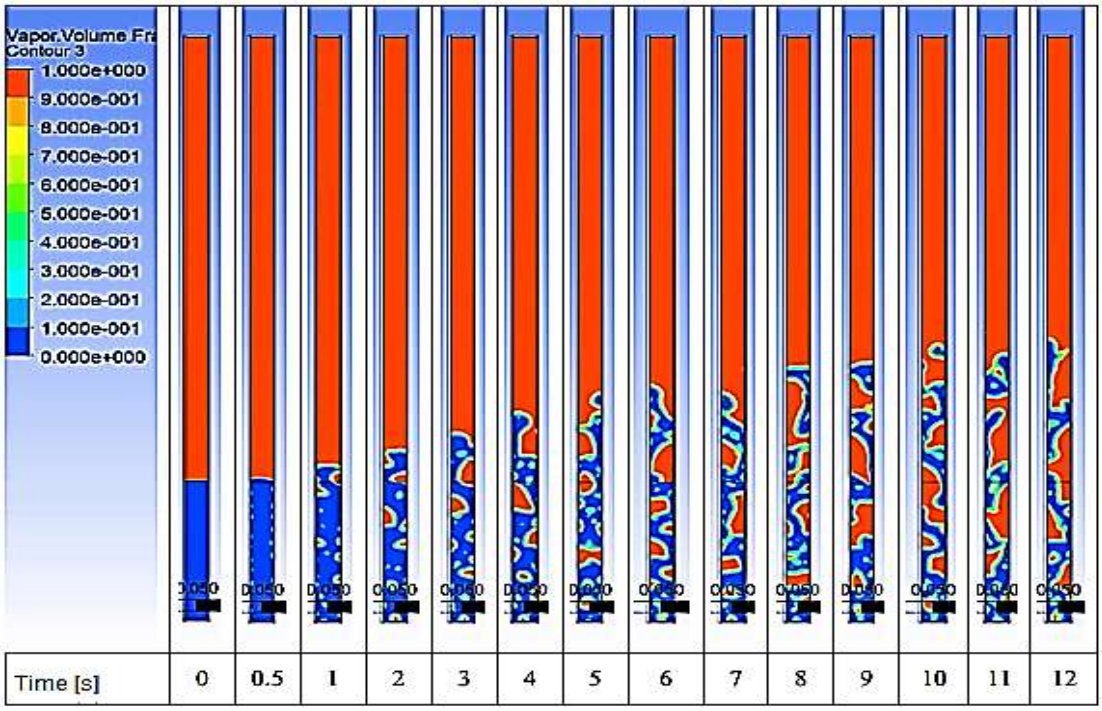

Figure (13): Contour of the Volumetric Ratio of Vapor – case 3.

Figure 14 shows the temperature distribution diagram over time on which the calculation of the equivalent thermal resistance of the tube is based, as in **Figure 15**, taking the value (0.309 [k/W]) at moment (10 [s]), and its decrease before that due to the liquid merging with the vapor masses, affected by the thermal gradient.

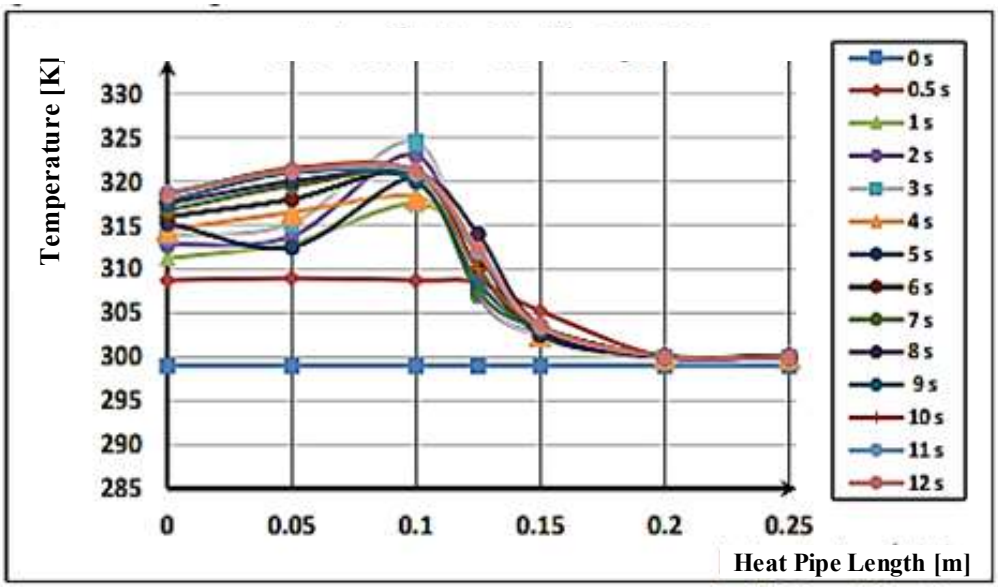

Figure (14): Temperature Distribution-Heat Pipe Length, case 3.

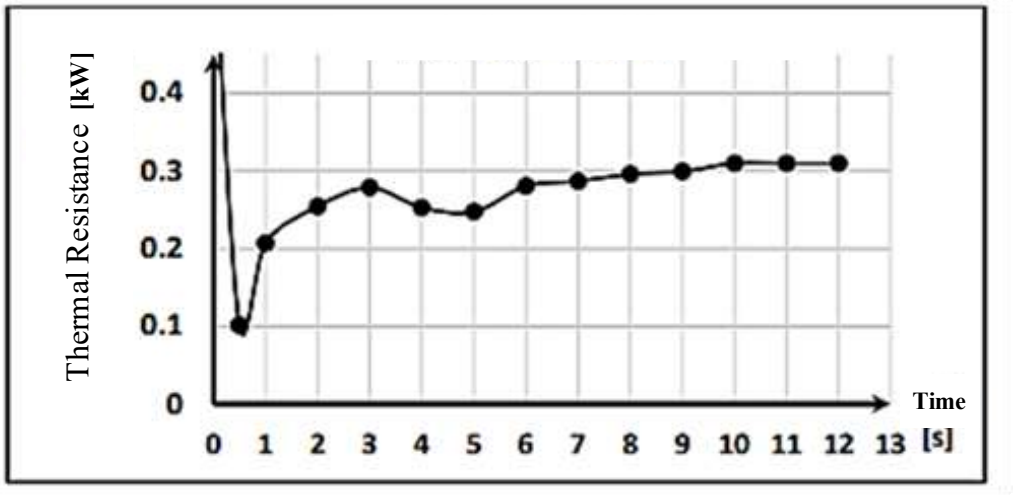

Figure (15): Equivalent Thermal Resistance - Time, case 3.

3.4 Comparison between Model Performances:

The equivalent thermal resistance was adopted for comparison between the selected models, which achieves equality between the ratio (L_e/d) and (L_c/d) in the numerical study, as shown in **Figure 16.** We find from **Figure 17**, which draws the relationship between the equivalent thermal resistance and the ratio of the pipe length to the diameter.

The thermal resistance decreases with the decrease in the ratio until it almost stabilizes, due to the different effect of each of the diameter and length on the processes of boiling, evaporation, and flow, which affect the heat transfer and its speed.

From **Figure 18**, which draws the relationship between the equivalent thermal resistance and the ratio of the evaporator length to the diameter, we find that the thermal resistance decreases as it decreases until it almost stabilizes due to the different effects of each of the diameter and the evaporator on the heating area and the rate of heat transfer.

The effect of the filling ratio plays the same role as in **Figure 19**, where the models achieve an average filling ratio of the evaporator volume and follow the evaporator surface temperature.

Based on this comparison between the three models, the diagrams resulting from the numerical study, and the perceptions provided by the contours of the phase ratio and the heat pipe temperature, it is clear that heat pipe performance follows the equivalent thermal resistance and the time to reach steady state operation.

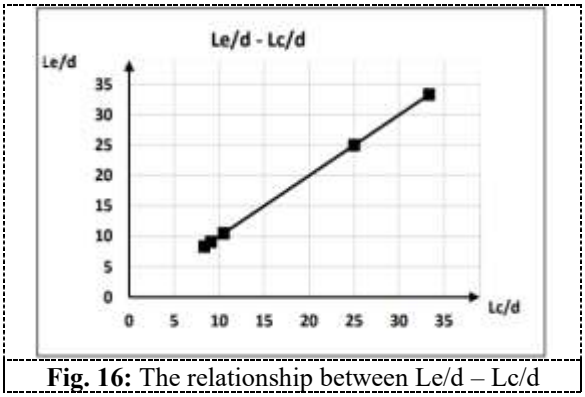

Fig. 16: The relationship between Le/d – Lc/d

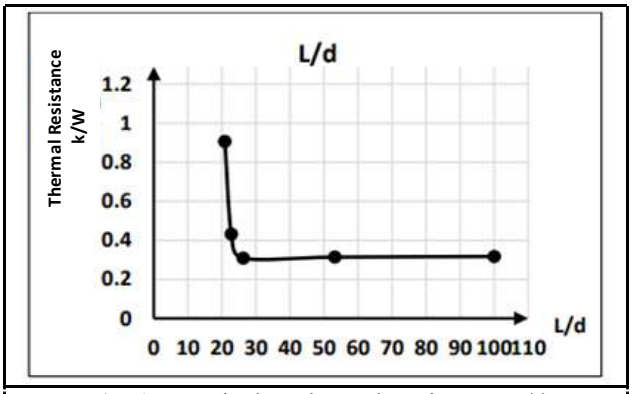

Fig. 17: Equivalent thermal Resistance L/d

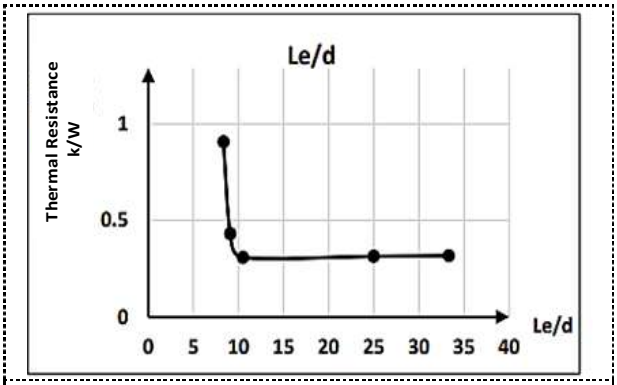

Fig. 18: Equivalent thermal Resistance Le/d

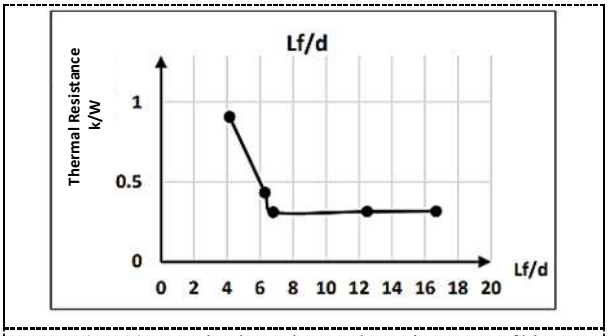

Fig. 19: Equivalent thermal Resistance Lf/d

4. Conclusions

This study presents a numerical investigation of thermosyphon heat pipe thermal performance, focusing on the effects of tube diameter, fill ratio, and geometric ratios on heat transfer and thermal resistance. The main findings are as follows:

1. The thermosyphon reaches stable operation as temperatures and equivalent thermal resistance stabilize, confirming effective heat transfer.
2. Optimal performance is achieved at a fill ratio of 70%, minimizing thermal resistance. Deviations from this value increase resistance by 18–25%.
3. Geometric dimensions significantly influence performance:
    - Smaller diameter tubes are 12% more efficient than larger ones, due to faster vapor movement and lower thermal resistance.
    - Increasing tube diameter or fill ratio increases start-up time by 25–40%, while higher evaporator heat flux reduces start-up time by 35%.
4. Thermal resistance behavior:
    - Increasing heat transfer rate by 50% reduces thermal resistance by 15%.
    - Exceeding the optimum liquid-column-height-to-diameter ratio increases thermal resistance by 20%.

5.The paper has established that length to diameter ratios, liquid column height to diameter ratio, and the correct heat flux management is vital in achieving maximum thermal efficiency. The increase of evaporator area in small diameter tubes does not reduce stability but enhances performance.

These findings, in general, are quantitative design and optimization advice to the thermosyphon heat pipes, and have direct applications in cooling of electronics, solar energy systems, and thermal management of batteries. This systemic study of the geometric and operational parameters provides an operational model of future heat pipes design, which would enable the enhancement of heat transfer but reduce thermal resistance.

References

[1] S. J. Ali, J. M. Jalil, and A. L. Shuraiji, “Performance enhancement of evacuated tube solar collectors: A review,” *Engineering and Technology Journal*, 2025. doi: 10.30684/etj.2025.155236.1853.

[2] U. Sharma, "A study of high temperature heat pipes and the impact of magnetic field on the flow of liquid metal," M.Sc. thesis, Michigan Technological University, MI, USA, 2021. doi: 10.37099/mtu.dc.etdr/381.
[3] N. J. Gernert, *Heat Pipe Reliability Documentation*. Lancaster, PA, USA: Thermacore Inc., 1999, pp. 1–21.
[4] A. Faghri, "Heat pipes: Review, opportunities and challenges," *Frontiers in Heat Pipes*, vol. 5, no. 1, 2014.
[5] D. Reay and A. Kew, *Heat Pipes: Theory, Design and Applications*, 5th ed. Oxford, U.K.: Elsevier, 2006.
[6] G. M. Grover, T. P. Cotter, and G. F. Erickson, "Structures of very high thermal conductance," *Journal of Applied Physics*, vol. 35, p. 1990, 1990.
[7] G. P. Peterson, *An Introduction to Heat Pipes: Modeling, Testing, and Applications*. New York, NY, USA: Wiley, 1994.
[8] A. Faghri, *Heat Pipe Science and Technology*. New York, NY, USA: Taylor & Francis, 1995.
[9] I. Dincer, *Refrigeration Systems and Applications*. Chichester, U.K.: Wiley, 2003, pp. 319–354.
[10] C. R. Sonawane, P. Gole, and A. Pandey, "Numerical modelling of two-phase closed thermosyphon flexible heat pipe," in *Proc. 12th Int. Conf. Thermal Engineering: Theory and Applications*, Gandhinagar, India, Feb. 23–26, 2019.
[11] M. Badache, Z. Aidoun, P. Eslami-Nejad, and D. Blessent, "Ground-coupled natural circulating device (thermosiphon): A review of modeling, experimental and development studies," *Inventions*, vol. 4, no. 14, pp. 2–41, 2019.
[12] S. B. Riffat, X. Zhao, and P. S. Doherty, "Analytical and numerical simulation of the thermal performance of mini gravitational and micro gravitational heat pipes," *Applied Thermal Engineering*, vol. 22, pp. 1047–1068, 2002.
[13] P. Amatachaya and W. Srimuang, "Comparative heat transfer characteristics of a flat two-phase closed thermosyphon and a conventional two-phase closed thermosyphon," *International Journal of Heat and Mass Transfer*, vol. 37, p. 293, 2010.
[14] B. Fadhl, L. C. Wrobel, and H. Jouhara, "Numerical modelling of the temperature distribution in a two-phase closed thermosyphon," *WIT Transactions on Engineering Sciences*, vol. 83, pp. 377–387, 2014.
[15] F. Bandar, "Modelling of the thermal behavior of a two-phase closed thermosyphon," Ph.D. dissertation, Brunel Univ. London, U.K., 2015.
[16] K.-S. Ong and C. Lim, "Performance of water-filled thermosyphons between 30–150 °C," *Frontiers in Heat Pipes*, vol. 6, 2015.
[17] J. Strain, "Experimental comparison of heat pipes and thermosyphons containing methanol and acetone," B.Eng. thesis, Univ. of Victoria, Canada, 2017.
[18] Z. Zhao *et al.*, "Numerical study on the transient thermal performance of a two-phase closed thermosyphon," *Energies*, vol. 12, p. 80, 2019.
[19] B. Abdullahi *et al.*, "Experimental and numerical investigation of thermosyphon heat pipe performance at various inclination angles," *Journal of Advanced Research in Fluid Mechanics and Thermal Sciences*, vol. 44, no. 1, pp. 85–98, 2018.
[20] V. Kamburova, A. Ahmedov, L. K. Iliev, I. Beloev, and I. R. Pavlovic, "Numerical modelling of the operation of a two-phase thermosyphon," *Thermal Science*, vol. 22, no. 5, pp. 1311–1321, 2018.
[21] D. Gamboa and H. Bernardo, "Influence of turbulence, density, phase change, and phase interfaces models on the performance of the numerical simulation of a two-phase closed thermosyphon," *TecnoLógicas*, vol. 23, no. 49, pp. 53–70, 2020.
[22] A. B. Temimy, A. Abdulrasool, and F. A. Hamad, "Study of heat pipe thermal performance with internal modified geometry," *Fluids*, vol. 6, no. 231, pp. 1–24, 2021.
[23] G. Czerwinski and J. Wołoszyn, "Numerical study of a cooling system using phase change of a refrigerant in a thermosiphon," *Energies*, vol. 14, p. 3634, 2021.
[24] P. L. Anto and J. Varghese, "Three-dimensional steady-state numerical analysis of inclined two-phase closed thermosyphon for solar applications," *Case Studies in Thermal Engineering*, vol. 30, 101805, 2022.
[25] K. Wang, C. Hu, Y. Cai, Y. Li, and D. Tang, "Investigation of heat transfer and flow characteristics in two-phase loop thermosyphon by visualization experiments and CFD simulations," *International Journal of Heat and Mass Transfer*, vol. 203, 123812, 2023.
[26] Y. Cai, X. Hu, J. Lu, Y. Li, D. Tang, and C. Hu, "Impact of working fluid properties on heat transfer and flow characteristics of two-phase loop thermosyphon with high filling ratios," *International Journal of Heat and Mass Transfer*, vol. 238, 126482, 2025.
[27] M. Misale and I. Alem, "Numerical simulation of single-phase natural circulation loops," *International Journal of Heat and Mass Transfer*, vol. 131, pp. 865–889, 2019, doi: 10.1016/j.ijheatmasstransfer.2018.11.164.
[28] D. Gamboa and B. Herrera, "Influence of turbulence, density, phase change, and phase interfaces models on the performance of the numerical simulation of a two-phase closed thermosyphon," *TecnoLógicas*, vol. 23, no. 49, pp. 53–70, 2020. doi: 10.22430/22565337.1563.
[29] F. Kreith and R. F. Boehm, "Heat and mass transfer," in *Mechanical Engineering Handbook*. Boca Raton, FL, USA: CRC Press, 2000, pp. 261–271.
[30] N. Atabaki, "Experimental and computational studies of loop heat pipes," Ph.D. dissertation, McGill Univ., Montreal, QC, Canada, 2006.